Water Resour Manage (2010) 24:1065–1088
DOI 10.1007/s11269-009-9486-2

# Comparison of Process-Based and Temperature-Index Snowmelt Modeling in SWAT

**Bekele Debele · Raghavan Srinivasan · A. K. Gosain**

Received: 9 March 2008 / Accepted: 17 July 2009 /
Published online: 31 July 2009


**Abstract** Snowmelt hydrology is an important part of hydrological analyses where significant proportion of precipitation is expected to fall in a snow form. Many models have long been introduced to enable the simulation of snowmelt processes in the watershed ranging from simple temperature based equations to complex and sophisticated process-based equations. Usually, mixed results have been reported whether or not the difference between results achieved by incorporating data demanding models vis-à-vis simple temperature-index models is justifiable. In this study, we compared the performances of physically based energy budget and simpler temperature-index based snowmelt calculation approaches within the SWAT model at three sites in two different continents. The results indicate insignificant differences between the two approaches. The temperature-index based snowmelt computation method had the overall model efficiency coefficients ranging from 0.49 to 0.73 while the energy budget based approach had efficiency coefficients ranging from 0.33 to 0.59 only. The magnitude of the differences varied based on where the models were applied. However, comparison between two process-based snowmelt estimation procedures (with and without the inclusion of aspect and slope as factors dictating the incoming solar energy) indicate that accounting for ground surface slope and aspect in the snowmelt model slightly improved the results. We conclude that for most

B. Debele
Sustainable Development Department of the Middle East and North Africa Region,
World Bank, Washington, DC 20043, USA

B. Debele (✉)
1809 Locust Grove Road, Silver Spring, MD 20910, USA
e-mail: bd58@cornell.edu

R. Srinivasan
Spatial Sciences Laboratory, Texas A&M University, College Station, TX 77843, USA

A. K. Gosain
Department of Civil Engineering, Indian Institute of Technology, Hauz Khas,
New Delhi, 110 016, India

practical applications where net solar radiation, not turbulent heat flux, dominates the snowmelt dynamics, a simpler temperature-index snowmelt estimation model is sufficient.

**Keywords** Snow cover · Snowmelt · Solar radiation · SWAT · Temperature index

## 1 Introduction

Precipitation occurs in two different forms: (1) liquid precipitation, which is usually called rainfall, and (2) solid precipitation (snow). The power of any hydrological model used to simulate runoff from snowy watersheds depends on how well the model accounts for the processes of these precipitation types in the basin (Morid et al. 2002; Essery 2003; Valeo and Ho 2004). For example, the usual rainfall–runoff hydrological models, primarily developed to simulate runoff as a function of rainfall alone, are not sufficient to examine water resources issues in snowy river basins. Many hydrological models account for snowmelt by incorporating an additional snowmelt module into the rainfall–runoff simulation models (Cazorzi and Fontana 1996; Neitsch et al. 2001; Martinec et al. 2008; Rango and Martinec 2008; Rango and Dewalle 2008). Some of these models use simple temperature-based equations (Albert and Krajeski 1998; Neitsch et al. 2001; Debele and Srinivasan 2005) while others adopt sophisticated and process-based methods (Bathurst and Cooley 1996; Todini 1996; USACE 1998; Koivusalo and Kakkonen 2002) for snowmelt computation. Detailed review of the many methods of snowmelt computation was made elsewhere (Morid et al. 2001; Koivusalo and Kakkonen 2002). We examined two commonly used and widely adopted snowmelt computation approaches: temperature index based and energy budget based methods. We used the soil and water assessment tool (SWAT) model as a parent hydrological model in which these two snowmelt modules were studied.

The SWAT model (Arnold et al. 1996; Neitsch et al. 2001) is currently equipped with a snowmelt estimation procedure based on a simple temperature index approach. To account for orographic effects on precipitation, temperature and solar radiation, SWAT allows up to ten elevation bands to be defined in each subbasin (Neitsch et al. 2001). Accordingly, the snow accumulation, sublimation and melt are computed within each elevation band and weight-averaged subbasin wise. Snowmelt estimation based on the elevation band approach assumes that snowmelt depth in all subbasins within the same elevation band is constant. However, many argue that elevation is not the only variable that dictates snowmelt in a subbasin (Morid et al. 2001, 2002; LaMalfa and Ryle 2008). Among many other factors that influence snowmelt, land use/land cover, aspect and slope are the dominant ones (Morid et al. 2002; LaMalfa and Ryle 2008). For example, the angle of exposure of the land surface (aspect and slope) affects the amount of precipitation and its accumulation over a period of time. Similarly, the angle of exposure of the land surface to sunlight greatly affects the amount of energy absorbed, and hence the depth of snowmelt, leading to impacts on the growth of vegetation. Such in turn influences the hydrological processes in a given basin.

In addition, for any physically based hydrological model (e.g., SWAT), it will be inconsistent to adopt a physically based approach for one part of the analyses and a simple empirical method for another. For instance, SWAT provides its users with different alternatives of computing daily potential evapotranspiration (PET) ranging from a temperature index based Hargreaves–Samani method (Hargreaves and Samani 1985) to a physically based Penman–Monteith (Allen et al. 1998) approach. Thus, in SWAT applications with the combination of Green–Ampt for infiltration and Penman–Monteith for PET calculations, it is unrealistic to use a simple empirically based temperature-index approach for snowmelt calculation. Such inconsistence may eventually lead to unreasonable end results. Many would argue that a physically based energy-budget snowmelt calculation approach is an appropriate alternative. The objective of this study was therefore to examine if in fact the more detailed and process-based snowmelt computation following the energy budget approach is better than the existing default temperature index based method to better reproduce stream flows in the SWAT model.

### 1.1 Theory

The thermodynamics of snowmelt are well understood and have been described in various details (USACE 1956; Anderson 1968, 1973, 1976; Gray and Male 1981; Marks and Dozier 1992; Link and Marks 1999; Pomeroy et al. 2003; Martinec et al. 2008; Rango and Dewalle 2008). One of the most thorough studies ever undertaken was by the U.S. Army Corps of Engineers (USACE 1956), which is still often cited and regarded as a definitive work on the subject of snowmelt dynamics, as well as being a source of equations for practical modeling. Similar works of Anderson (1968) has also led to an operational model in use by the National Weather Service (Anderson 1973). More recently, however, energy balance snowmelt models have been developed to operate on a spatially distributed basis, taking advantage of geographic information systems (GIS) and spatial datasets of elevation, slope and aspect, vegetation, soils, and hydro-meteorological variables. These include the models of Marks et al. (1998, 1999), Tarboton and Luce (1996) and Valeo and Ho (2004), to mention but a few. According to such approach, the rate and quantity of snowmelt depends on the amount of energy added to the system (Koivusalo and Kakkonen 2002; Valeo and Ho 2004). Assuming all the heat fluxes towards the snowpack are considered positive and those away considered negative, the sum of these fluxes is equal to the change in heat content of the snowpack ($\Delta Q$) over a given time period. Mathematically, this is depicted by:

$$\Delta Q = Q_N + Q_H + Q_E + Q_M + Q_G \tag{1}$$

where $Q_N$, $Q_H$, $Q_E$, $Q_M$, and $Q_G$ are the net incoming solar radiation, the sensible heat transfer, the latent heat transfer, the heat transfer through advection, and the heat transfer across the snow–soil interface, respectively. The National Engineering Handbook (NEH 2004) estimates that $Q_N$ (controlled by terrain, season, cloud cover, shading, air temperature, humidity, latitude) in Eq. 1 has the lion's share (60–90%) of the overall heat flux, followed by a combined $Q_H + Q_E$ (5–40%), which is in turn controlled by temperature and humidity gradients and wind speed. $Q_M$ and $Q_G$ contribute only marginally (2–6% in total) to the overall energy dynamics of snowmelt. Therefore, it is apparent to know not only the total energy, but also which energy sources are dominant to be able to understand and describe the behavior (amount and timing) of snowmelt in a given situation.

## 1.2 Snowmelt Modeling

Two basic approaches are commonly used to model snowmelt, one of which is based on a simple temperature index approach with the assumption that temperature is a major driving force in snowmelt processes (Aizen et al. 1996; Albert and Krajeski 1998; Neitsch et al. 2001; Tanasienko and Chumbaev 2008). The other approach hypothesizes that temperature alone cannot adequately explain the processes of snowmelt (Marks et al. 1998, 1999; NEH 2004; Zhang et al. 2007). For example, in situations where a combination of warm temperature plus high humidity and wind speed prevail, sensible and latent heats become substantial, if not dominant, sources of energy for snowmelt, not the usual net incoming solar radiation. Such event is commonly known as rain-on-snow. Whereas the former approach is simpler and easier to use, the latter is data intensive and sometimes cannot be done because of inadequate data or unwarranted detail for the work at hand.

### *1.2.1 Snowmelt Estimation Using Temperature-Index Method*

One of the most commonly used models under this category is the sinusoidal equation similar to that adopted in the current SWAT model (Neitsch et al. 2001). This approach assumes that potential snowmelt rate varies between two ranges: maximum (assumed to occur on June 21st) and minimum (assumed to occur on December 21st) following the sinusoidal function based on the day of a year. It is given by:

$$\mathrm{Q_{tot}} = SM_{rate}\left[\frac{(T_{sp} + T_{\max})}{2} - T_{sb}\right] \tag{2}$$

where $\mathrm{Q_{tot}}$ is the snowmelt depth in the elevation band in equivalent millimeter [mme], $\mathrm{SM_{rate}}$ is the snowmelt rate factor [mme/°C], $\mathrm{T_{sp}}$ is the daily snowpack temperature in the elevation band [°C], $\mathrm{T_{max}}$ is the maximum temperature of the day in the elevation band [°C], and $\mathrm{T_{sb}}$ is the snowmelt base temperature, which is the mean air temperature at which snowmelt will occur [°C]. The daily snowpack temperature is given by:

$$T_{snow(dn)} = T_{snow(dn-1)}(1 - \lambda sno) + T_{av}\lambda sno \tag{3}$$

where $\mathrm{T_{snow(dn)}}$ is the snowpack temperature on a given day [°C], $\mathrm{T_{snow(dn-1)}}$ is the snowpack temperature of a previous day [°C], $\lambda sno$ is the snow temperature lag factor [–], and $\mathrm{T_{av}}$ is the mean air temperature of the current day [°C]. As $\lambda sno$ approaches 1.0, the mean air temperature on the current day exerts an increasingly greater influence on the snowpack temperature, and the snowpack temperature from the previous day exerts less and less influence. The snowpack will not melt until the snowpack temperature exceeds a threshold value, $\mathrm{T_{sb}}$, which is specified by the user.

The snowmelt rate factor ($\mathrm{SM_{rate}}$) is in turn given by:

$$SM_{rate} = \frac{(SM_{\max} + SM_{\min})}{2} + \sin\left(\frac{j - 81}{58.09}\right)\frac{(SM_{\max} - SM_{\min})}{2} \tag{4}$$

where $\mathrm{SM_{max}}$ is the maximum melt rate for snow during a year (assumed to occur on June 21st) [mm/°C/day], $\mathrm{SM_{min}}$ is the minimum snowmelt rate during a year (assumed to occur on December 21st) [mm/°C/day], and j is the day of a year starting from January 1st and ranges from 1 through 365/366 based on whether or not the year is a leap year. In the default SWAT model, the values of $SM_{max}$, $SM_{min}$ and $T_{sb}$ are calibration parameters and can easily be adjusted for better model performance (Table 1).

The opponents of this approach argue that the snowmelt rate factor ($SM_{rate}$) and other associated model parameters, such as $SM_{max}$, $SM_{min}$ and $T_{sb}$ are site-specific and should be rigorously calibrated for use. In addition, such empirically based snowmelt modeling approach is less applicable when separation of snow surface energy fluxes (such as those described in Eq. 1, above) and prediction of the snow surface temperature are important, which is often the case when hydrological models are coupled with atmospheric models (Marshall et al. 1999). Also, under rain-on-snow conditions, such modeling endeavor is incompetent given that temperature alone cannot explain the snowmelt processes under such conditions (see Section 1.2). In addition, many (Koivusalo and Kakkonen 2002) argue that physically based snowmelt modeling approaches are also important to examine the impacts of land use changes on hydrological processes. For instance, commonly used temperature index (including energy budget based ones without some modifications to the short and long wave radiation fluxes, and sensible and latent heat turbulent transfers) snowmelt models are incapable to simulate snowmelt processes in forested watersheds. However, employing physically-based models with elaborate snowmelt dynamics, one can simulate the effects of land use changes (forest to other land use types, or vice-versa) on subsequent hydrological processes.

### *1.2.2 Snowmelt Estimation Following the Energy Budget Approach*

Snowmelt computation using the energy budget approach follows from accounting for the energy balance at the ground surface. It considers all the incoming, outgoing and stored energies, and finally determines the net incoming energy. If the net incoming energy is positive, this adds heat to the system and eventually leads to

**Table 1** List of parameters and corresponding values adopted in the default SWAT2K snowmelt module

| SWAT2K variable | Description | Range min, max | Value adopted |
|---|---|---|---|
| SFTMP | Snowfall temperature [°C] | −5, +5 | 0.0 |
| SNOEB | Initial snow water content in elevation band [mm] | 0, 300 | 0.0 |
| SMTMP | Snow melt base temperature [°C] | −5, +5 | 4.0 |
| TIMP | Snow pack temperature lag factor [–] | 0, 1 | 1.0 |
| SMFMN | Melt factor for snow on December 21st [mm H2O/°C day] | 0, 10 | 5.5 |
| SMFMX | Melt factor for snow on June 21st [mm H2O/°C day] | 0, 10 | 6.5 |
| SNOCOVMX | Minimum snow water content that corresponds to 100% snow cover [mm] | 0, 500 | 400.0 |
| SNO50COV | Fraction of snow volume represented by SNOCOVMX that corresponds to 50% snow cover [–] | 0, 1 | 0.5 |

melting of the snowpack. The rate and quantity of snowmelt depends on the amount of energy added to the system (Koivusalo and Kakkonen 2002; Valeo and Ho 2004; Sui and Koehler 2007; Zhao et al. 2009). Following from this approach, the amount of snowmelt ($Q_{Tot}$) in equivalent millimeter of water (mme) is computed by the following expression:

$$Q_{tot} = 0.0029875 \ \left(Q_N + Q_H + Q_E + Q_M + Q_G - \Delta Q_I\right) \tag{5}$$

where $\Delta Q_I$ is the rate of change in the internal energy stored in the snowpack [KJ/m$^2$] and other terms are defined similar to those under Eq. 1 [KJ/m$^2$]. The heat transfer across the snow–soil interface, $Q_G$, is usually assumed constant (~173 KJ/m$^2$) for various practical applications (US Army Corps of Engineers 1960; Walter et al. 2005). The constant 0.0029875 is a conversion factor from KJ/m$^2$ to equivalent millimeter (mme) of snowmelt. An accurate method of estimating snowmelt depth would be to measure each energy flux in Eq. 5. However, due to lack of such data, many resort to estimating the fluxes themselves using easily available data, such as temperature, geographic latitude, altitude and longitude, and DEM, all of which are readily available throughout much of the world. These are described in detail below.

1. The net solar radiation flux into the snowpack ($Q_n$) is estimated using the following expressions:

$$Q_n = R_s(1 - \text{alb}) + R_L \qquad \text{for open surfaces, and} \tag{6a}$$

$$Q_n = R_s\left[\tau_c(1 - f_s) + f_s\right](1 - \text{alb}) + R_L \qquad \text{for surfaces covered by conopy} \tag{6b}$$

where $R_s$, $R_L$, and alb are the incoming solar radiation on a plane perpendicular to the solar rays [KJ/m$^2$], net thermal heat transfer through longwave radiation [KJ/m$^2$], and albedo of the snow covered land [–], respectively; and $\tau_c$, and $f_s$ are the transmittance [–] and the sky-view fraction [–], respectively (Koivusalo et al. 2001; Koivusalo and Kakkonen 2002; Rasmus et al. 2008). The sky-view fraction is defined as the fraction of area above the ground unobstructed by the canopy. Snow albedo generally decreases with time (Wigmosta et al. 1994). We approximated the temporal decay of the snow albedo using the following expression:

$$\text{alb} = 0.43\left\{1 + \exp[-(K_e t)]\right\} \tag{7}$$

where $K_e$ and t are the snow albedo decay constant [~0.2 day$^{-1}$], and time elapsed since the last snowfall [days], respectively. We set the value of t to restart (t = 0) whenever fresh snowfall depth was more than 2 mm (as water equivalent) since the new snow covers the darker low albedo snow (McKay and Gray 1981; Tarboton and Luce 1996; Koivusalo and Kakkonen 2002). The incoming solar radiation on a horizontal plane ($R_s$) was determined following the Hargreaves–Samani temperature difference approach (Hargreaves and Samani 1985), and given by:

$$R_s = 0.18 R_a \left(T_{max} - T_{min}\right)^{0.5} \tag{8}$$

where $R_a$, $T_{max}$ and $T_{min}$ are the extraterrestrial solar radiation [KJ/m$^2$], maximum and minimum daily air temperatures [°C], respectively. $R_s$ in the form of Eq. 8 is assumed to have accounted for atmospheric transmissivity (Allen et al. 1998). The extraterrestrial solar radiation ($R_a$) is in turn given by:

$$R_a = \frac{r_0}{\pi}\left\{\cos^{-1}(-\tan\delta\tan\phi)\sin\delta\sin\phi + \cos\delta\cos\phi\sin\left[\cos^{-1}(-\tan\delta\tan\phi)\right]\right\} \quad (9)$$

where $r_0$ is the solar constant [~117.5 KJ/m$^2$ day], $\phi$ is the latitude of a location [radians], and $\delta$ is the solar declination [radians]. The solar declination ($\delta$) can be calculated using the day of a year as:

$$\delta = 0.4102\,\sin\left(\frac{2\pi}{365}(j-80)\right) \quad (10)$$

We calculated the net thermal heat flux through longwave radiation ($R_L$) for two different conditions:

1. for open surfaces:

$$R_L = \sigma\left\{\varepsilon_a T_{ak}^4 - \varepsilon_{sn} T_{snk}^4\right\}\left(0.34 - 0.14\sqrt{e_a}\right)(1.3n - 0.35) \quad (11a)$$

and

2. for surfaces covered by canopy (after Koivusalo and Kakkonen 2002):

$$R_L = \sigma\left\{f_s\varepsilon_a T_{ak}^4 - \varepsilon_{sn} T_{snk}^4 + (1 - f_s)\varepsilon_c T_c^4\right\}\left(0.34 - 0.14\sqrt{e_a}\right)(1.35n - 0.35) \quad (11b)$$

where $\varepsilon_a$, $\varepsilon_{sn}$, $\varepsilon_c$ are the emissivity of air, snow, and canopy surfaces, respectively; $T_{ak}$, $T_{snk}$, and $T_c$ are the air, snow, and canopy surface temperatures [K], respectively; and $e_a$, n and $\sigma$ are the air vapor pressure [mbar], the ratio of actual hour of sunshine to potential hour of sunshine [–], and the Stefan-Boltzman constant [~4.903 × 10$^{-6}$ KJ/day m$^2$ K$^{-4}$], respectively. We assumed the emissivity of snow to be ($\varepsilon_{sn}$ ~ 0.99) and that of canopy to be ($\varepsilon_c$ ~ 1.00). Whereas, the emissivity of the atmospheric air ($\varepsilon_a$) was determined by the following equation (after Herzfeld 1996):

$$\varepsilon_a = 9.2^{*}10^{-6}T_{ak}^2 \quad (12)$$

And n is given by:

$$n = 2\left[\frac{R_s}{R_a} - 0.25\right] \quad (13)$$

The last two terms on the RHS of Eqs. 11a and 11b, $\left(0.34 - 0.14\sqrt{e_a}\right)$ and $(1.35n-0.35)$, are correction coefficients for air humidity and cloudiness, respectively. Some studies exclude the correction factors from the emission part (Imberger and Patterson 1981), while others use them for both emission and absorption terms (Herzfeld 1996). However, Hodges (1998) and Allen et al. (1998) stressed that the inclusion of the correction terms (air humidity and cloudiness) for both emission and absorption gives better estimates of the net heat transfer through longwave radiation. We have included both coefficients in our study.

2. The energy exchanges through turbulent heat flux (sensible heat flux, $Q_H$, and latent heat flux, $Q_E$) are estimated as follows:

$$Q_H = \left(\frac{C_a}{r_h} + E_{HO}\right)(T_a - T_{sn}) \quad (14)$$

where $Q_H$ is the sensible heat transfer [KJ/m$^2$]; $E_{HO}$ is the windless convection coefficient for the sensible heat flux [~172.8 KJ/m$^2$/°C]; $C_a$ is the heat capacity of the air [~1.29 KJ/m$^3$ °C]; $T_a$ and $T_{sn}$ are the air and snow surface temperatures [°C], respectively; and $r_h$ is the aerodynamic resistance to the turbulent heat exchange [day/m]. The aerodynamic resistance is usually determined following the eddy diffusion theory assuming equal resistances to transfer of heat, vapor, and momentum. Many (Male and Granger 1981; Brutsaert 1982) disqualify this assumption to be strictly true. However, it has been commonly used in hydrological applications with minimal effects (Calder 1990; Wigmosta et al. 1994; Lundberg et al. 1998; Koivusalo and Kakkonen 2002). We estimated the resistance to the turbulent heat exchange above the snowpack ($r_{he}$) using the following equations:

$$r_{he} = r_a + r_c + r_s \qquad \text{for forested areas, and} \tag{15a}$$

$$r_{he} = r_s \qquad \text{for open areas} \tag{15b}$$

where $r_a$, $r_c$, and $r_s$ are the aerodynamic resistance to vapor transport above the canopy, the resistance within the canopy, and the resistance between the snow surface and the measurement height for meteorological data ($Z_{rs} \sim 2$m), respectively [day/m]. The aerodynamic resistance to vapor transport above the canopy ($r_a$) is in turn given by:

$$r_a = \frac{1}{86400}\left\{\frac{1}{k^2 u_r}\ln\left(\frac{Z_r - d_0}{Z_{Oc}}\right)\ln\left(\frac{Z_r - d_0}{h_0 - d_0}\right) + \frac{h_0}{mK_h}\left[e^{n-n(Z_{Oc}+d_0)/h_0} - 1\right]\right\}, \tag{16}$$

where

$$K_h = \frac{u_r k^2 (h_0 - d_0)}{\ln\left(\frac{Z_r - d_0}{Z_{Oc}}\right)} \tag{17}$$

where k is the von Karman constant (~0.41) [–], $u_r$ is the wind speed measured at reference height, $Z_r$ [m/s], $d_0$ is the zero-plane displacement height (~0.63$h_0$) [m], $Z_{Oc}$ is the roughness length of the canopy (~0.13$h_0$) [m], $h_0$ is the vegetation height [m], m is an extinction coefficient [–], and $K_h$ is the logarithmic diffusion coefficient at the top of the canopy [m$^2$/s]. Similarly, resistances $r_c$ and $r_s$ are also given by:

$$r_c = \frac{h_0 e^m}{mK_h}\left[e^{-mZ_{rs}/h_0} - e^{-m(d_0+Z_{o0})/h_0}\right]\frac{1}{86400}, \tag{18}$$

and

$$r_s = \frac{\left[\ln\left(\frac{Z_{rs} - d_s}{Z_{os}}\right)\right]^2}{k^2 u_{rs}}\frac{1}{86400} \tag{19}$$

where $d_s$ is the depth of the snowpack [m], $Z_{os}$ is the snow surface roughness length [m], and $u_{rs}$ is the wind speed at $Z_{rs}$ [m/s]. We have also adjusted the aerodynamic resistance ($r_{he}$) by calculating the corrections for stable and unstable atmospheric conditions following the Choudhury and Monteith's (1988) approach.

$$r_h = r_{he}/(1 - 5\text{Ri})^2 \qquad \text{for stable conditions: } 0 < \text{Ri} \le \text{Ri}_{max} \tag{20a}$$

$$r_h = r_{he}/(1-5\mathrm{Ri})^{\frac{3}{4}} \qquad \text{for unstable conditions: } Ri < 0, \tag{20b}$$

where

$$\mathrm{Ri} = \frac{g(T_a - T_{sn})(Z_{rs} - d_s)}{u_{rs}^2\left[0.5(T_a + T_{sn}) + 273.15\right]} \tag{21}$$

where Ri and $\mathrm{Ri}_{max}$ are the estimate and the upper limit of the Richardson number (~0.16), respectively [–], and g is the acceleration due to gravity [~9.81m/s$^2$].

The latent heat exchange ($Q_E$), similar to the sensible heat transfer, depends on turbulence of the air. Assuming that turbulent transfer coefficients for heat and vapor are equal, latent heat transfer can be obtained using the Bowen ratio (Bowen 1926; Anderson 1973), and can be expressed as:

$$\frac{Q_H}{Q_E} = \gamma \frac{T_a - T_{sn}}{e_a - e_o} \tag{22}$$

where $Q_E$ is the heat flux due to vaporization and condensation [KJ/m$^2$], $\gamma$ is the psychrometric constant [mbar/°C] ($\gamma = 0.00057P_a$, where $P_a$ is the atmospheric pressure [mbar]), $e_a$ is the actual vapor pressure of the air [mbar], and $e_o$ is the vapor pressure at the snow surface [mbar] (assumed equal to the saturation vapor pressure at the snow temperature). The saturation vapor pressure at a snow surface temperature ($T_{sn}$) is given by (after Allen et al. 1998):

$$e_s = 0.6108 \exp\left(\frac{17.27 T_{sn}}{T_{sn} + 237.3}\right) \tag{23}$$

Whereas, the actual air vapor pressure ($e_a$) is estimated by:

$$e_a = e_{as}\frac{RH}{100} \tag{24}$$

where $e_a$ is the actual vapor pressure at a given air temperature [mbar], RH is the relative humidity [%], and $e_{as}$ is the saturated vapor pressure at a given air temperature [mbar], computed using Eq. 23 with air temperature substituted for snow surface temperature.

3. The heat transfer by mass change ($Q_M$) is the advective heat added by means of rainfall, and is computed following:

$$Q_M = \frac{C_p \rho_w P(T_r - T_{sn})}{10^3} \tag{25}$$

where $Q_M$ is the heat transfer through advection [KJ/m$^2$], $C_p$ is the specific heat capacity of rainwater [~4.18 KJ/kg °C], $\rho_w$ is the density of water [~1,000 kg/m$^3$], P is rainfall quantity [mm/day], and $T_r$ is the rainwater temperature [°C]. We assumed that the rainwater temperature is equal to the wet-bulb temperature.

4. We also computed the change in internal energy of the snowpack ($Q_i$) and the heat deficit ($\Delta Q_i$) reduced by the heat released when melt or rainwater freezes within the snow cover following:

$$Q_I = d_s\left(C_{pi}\rho_i + C_{pl}\rho_l + C_{pv}\rho_v\right) T_{sn} \tag{26}$$

where $Q_I$ is the internal energy of the snowpack (after Gray and Prowse 1992) [KJ/m$^2$]; $d_s$ is the snow depth [m]; $\rho_i$, $\rho_l$ and $\rho_v$ are the density of ice [~922 kg/m$^3$], liquid rain [$\sim$1,000 kg/m$^3$], and vapor [$\sim$4.885E$-$3 kg/m$^3$], respectively; and $C_{pi}$, $C_{pl}$, and $C_{pv}$ are the specific heat capacity of ice [$\sim$2.1 KJ/kg °C], liquid water [$\sim$4.18 KJ/kg °C], and vapor [1.976 KJ/kg °C], respectively. We assumed that the contribution from the vapor phase is negligible. The rate of change in the internal energy stored in the snowpack ($\Delta Q_i$) is given by:

$$\Delta Q_I = (Q_I)_t - (Q_I)_{t-1} \tag{27}$$

where $\Delta Q_I$, $(Q_I)_t$, $(Q_I)_{t-1}$, are the rate of change in the internal energy stored in the snowpack, and the internal energy stored in the snowpack on the current day (t) and previous day (t $-$ 1), respectively [KJ/m$^2$]. If the heat deficit of the snowpack ($\Delta Q_i$) is positive, the snowpack's temperature is below freezing. This phenomenon is prominent during diurnal temperature cycles with refreezing at night because of radiational cooling.

### *1.2.3 Estimation of Solar Radiation on Inclined Surfaces (The SWIFT Algorithm)*

This method adjusts the incoming solar radiation on a horizontal surface at ground level, accounting for the variations in slope and aspect of the land surface. This algorithm is designed based on the hypothesis that land surfaces with westerly inclining aspect and steeper slopes stay under shadow from direct solar radiation during the mornings and vice versa during the afternoons, and therefore accordingly affecting the rate of snowmelt. With the same token, easterly inclining portions of the watershed will receive direct sunlight energy during the mornings and less during the afternoons based on the angle of surface inclination. It is given by:

$$R_s = \cos(i) R_\perp \tag{28}$$

where $R_\perp$ is the incoming solar radiation on a surface which is perpendicular to the solar rays (determined using Eq. 8; the Hargreaves–Samani method in this study), and cos(i) is the adjustment factor for inclined surfaces other than horizontal. We used similar procedures to that of Anderson (1973) (Swift 1976; Cazorzi and Fontana 1996) to calculate the adjustment factor (cos(i)), given by:

$$\cos(i) = \cos(a_s)\cos(\xi) + \sin(a_s)\sin(\xi)\cos(\psi - \psi_s) \tag{29}$$

where $a_s$ is the slope angle of the land surface [°], $\xi$ is the zenith angle [°], $\psi$ is the azimuth angle of the sun [°], and $\psi_s$ is the slope aspect measured from north [°]. Details of how to estimate for the variables given under Eq. 29 can be found in most textbooks and papers dealing with solar radiation and shading (McKenny et al. 1999; Wilson and Gallant 2000; Becker 2001; LaMalfa and Ryle 2008).

## 2 Methods

### 2.1 Model Setup

The Soil and Water Assessment Tool (SWAT model version 2000—SWAT2K) was used as the background hydrological model to evaluate the implications of different snowmelt simulation modules on the overall basin hydrology. The default SWAT2K is equipped with a snowmelt module that estimates snowmelt using a temperature-index approach based on elevation band (dividing a given basin into up to ten elevation bands). We also added additional snowmelt module to SWAT2K representing snowmelt processes based on the energy-budget approach (SNOWBP) employing Eqs. 5 through 29. The new SNOWBP snowmelt module computes snowmelt following the energy budget approach using both elevation band (BAND) and pixel-by-pixel (PIXEL) as a basis for snowmelt calculation.

The SWAT model was then ran under three different snowmelt calculation scenarios: (1) using a default temperature-index approach with elevation band as a unit of snowmelt computation (SWAT2K), (2) using energy-budget approach with elevation band as a unit of snowmelt estimation (BAND), and (3) using energy-budget approach with pixel as a unit of snowmelt calculation (PIXEL). In the case of snowmelt computation following the pixel-wise approach (PIXEL), the incoming solar radiation was modified following the approaches used in the SWIFT algorithm (Cazorzi and Fontana 1996), taking into account the slope and aspect of the land surface (see "Estimation of Solar Radiation on Inclined Surfaces (the SWIFT algorithm)" for details). Conversely, under the BAND scenario, the incoming solar radiation on a horizontal plane at the ground surface was assumed to be uniformly distributed in each elevation band despite the differences in slope and aspect within the elevation band.

One of the visible advantages of the SNOWBP module as opposed to the SWAT2K snowmelt module is that the SNOWBP module was designed in such a way that different energy balance calculation equations apply for different types of land cover. For instance, the equations used to calculate the net solar radiation flux and net thermal heat flux through longwave radiation are different for forest covered and barren lands—the facility that is nonexistent in the default SWAT2K snowmelt module. In addition, in order to take advantage of the physically based module in the SNOWBP and account for the dynamic diurnal variation of snowmelt processes, we allowed the SWAT model to compute energy balances, and thus snowmelt, on hourly basis but accumulate snowmelt depths on daily basis for routing purposes. Hourly temperature and solar radiation data for such use were generated from daily corresponding data series following a widely used cosine function (Neitsch et al. 2001; Green and Kozek 2003; Debele et al. 2007).

After setting up the SWAT model under three different snowmelt calculation scenarios, we calibrated the model parameters (especially those related to snowmelt calculation) under each scenario until after observed and calibrated runoff values reasonably matched. That is, we adopted optimum values for sensitive parameters in each snowmelt estimation module for comparison. The values of parameters adopted for snowmelt computation following the default SWAT2K and SNOWBP modules are depicted in Tables 1 and 2, respectively. The most sensitive parameters in the default SWAT2K snowmelt module are the snowmelt rate factors SMFMN and SMFMX (Table 1). Similarly, the most sensitive parameter in the SNOWBP module is the value of the threshold snow temperature to distinguish liquid from solid rain (TDSL) (Todini 1996; Debele and Srinivasan 2005; Manohar et al. 2008).

## 2.2 Study Area and Input Data

We used data from three watersheds in two different countries (two from Montana in the US, and one from the Yellow River basin in China) (Figs. 1 and 2). Figures 1 and

**Table 2** List of parameters and corresponding values adopted in the energy-based snowmelt computation module (SNOWBP)

| SNOWBP variable | Description | Range min, max | Value adopted |
|---|---|---|---|
| SKYV | Sky-view fraction [–] | 0.1, 0.2 | 0.15 |
| TRAN | Transmittance [mm] | 0.0, 0.1 | 0.0 |
| EXTC | The extinction coefficient | ±10% | 1.9 |
| SROS | The snow surface roughness length [m] | ±5% | 0.005 |
| SROC | The canopy surface roughness length [m] | ±5% | $0.13h_0$ |
| ZPDH | Zero-plane displacement height [m] | ±5% | $0.63h_0$ |
| TDSL | The threshold snow temperature to distinguish liquid from solid rain [°C] | −2, +2 | 2.0 |
| ALDC | The snow albedo decay constant [day$^{-1}$] | 0.15, 0.25 | 0.2 |

2 depict the boundaries and land use/land cover descriptions of the watersheds. In addition, Tables 3 and 4 describe the general characteristics (area, elevation, latitude, longitude), and percent distribution by area of the watersheds using slope steepness and aspect. The major land use/land cover type in the Tuchuck Creek watershed is forest cover (64%), followed by barren land (18%) and residential areas (11%) while the entire watershed area of Tenderfoot is forest cover (Fig. 1). On the other hand, from Fig. 2 the majority land cover in the Dashui watershed is pastureland (88%), followed by wetland (8%) and rangeland (3%)

From Table 3, the majority portion of the Tuchuck Creek watershed is comprised of steep slopes. About 59% of the watershed has slopes greater than 35° steepness, compared with Tenderfoot (3.6%) and Dashui (0.01%) watersheds. On the contrary, the majority portion of the Tenderfoot and Dashui watersheds are comprised of

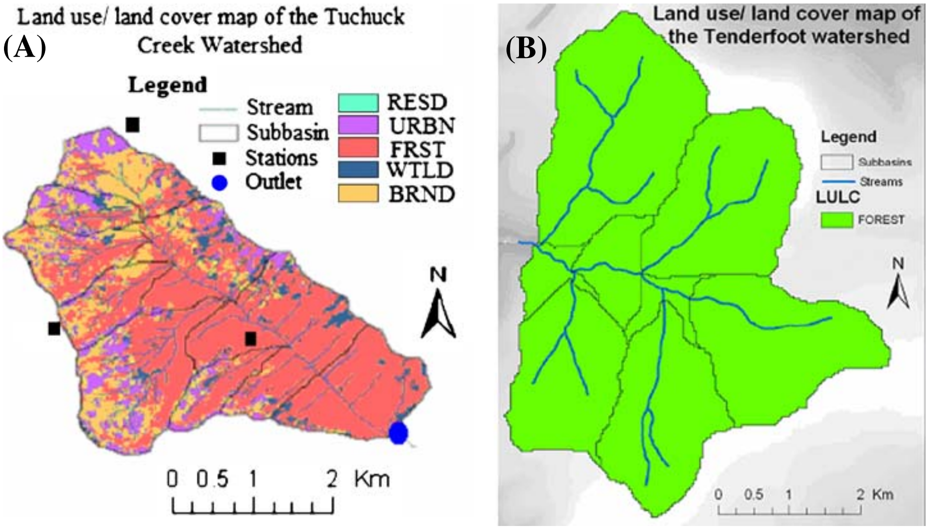


**Fig. 1** Land use/land cover map, watershed boundary and stream network of the Tuchuck Creek watershed (**a**) and Tenderfoot watershed (**b**), MT, USA; *RESD*, *URBN*, *FRST*, *WTLD* and *BRND* stand for residential, urban, forest, wetland and barren land use/land cover categories, respectively

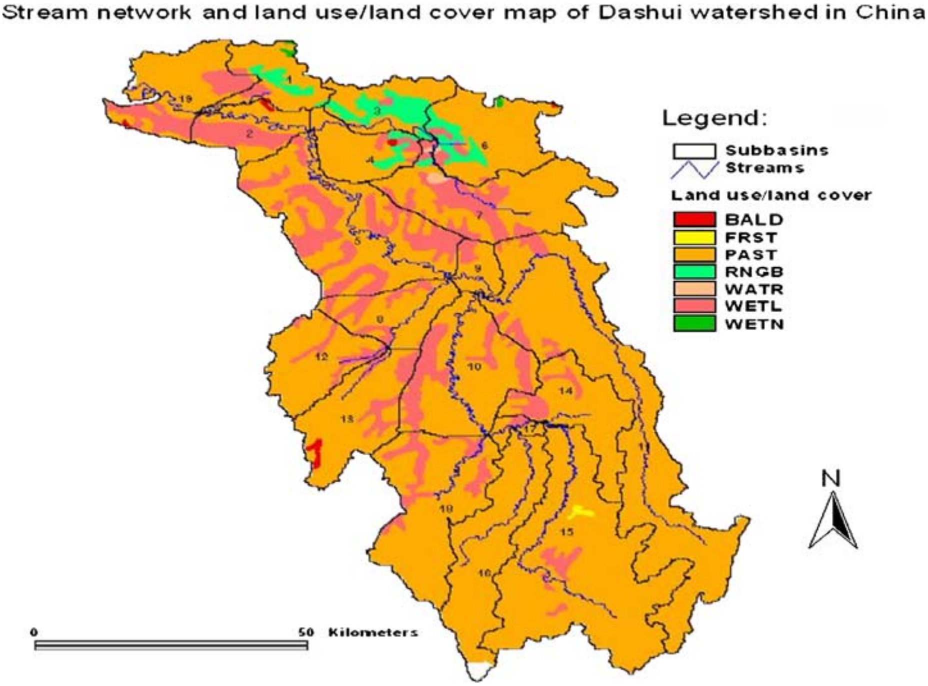


**Fig. 2** Land use/land cover map, watershed boundary and stream network of the Dashui watershed, Yellow River basin, China; *BALD*, *FRST*, *PAST*, *RNGB*, *WATR*, *WETL* and *WETN* stand for bald, forest, pasture, rangeland, water, mixed wetland, and non-forested wetland land use/land cover categories, respectively

flat slopes—about 80% and 99% of the watersheds, respectively, have slopes less than 20° steepness. According to Table 4, more than 42% of the total area in the Tenderfoot watershed has westerly inclinations as opposed to Tuchuck (32%) and Dashui (only 17%). Conversely, the Tuchuck Creek watershed has the majority of its portion inclining towards the easterly direction (47%) as opposed to Tenderfoot (30%) and Dashui (only 16%) watersheds.

Data (such as soils, land use/land cover, weather, topography, and stream flow) used for analyses in this manuscript were obtained from various sources (Table 5). Daily precipitation and temperature data were obtained for the US watersheds (Tuchuk—from 1985 to 1988; and Tenderfoot—from 1995 to 2000) and Chinese watershed (Dashui—from 1991 to 1998). The first year data in each watershed were

**Table 3** General characteristics and percent distribution of watershed areas by slope steepness

| Slope steepness | Percent area cover | | | Watershed | Tuchuck | Tenderfoot | Dashui |
|---|---|---|---|---|---|---|---|
| [degree] | Tuchuck | Tenderfoot | Dashui | name | | | |
| <20 | 18.3 | 80.3 | 98.62 | Area [km$^2$] | 26.03 | 22.28 | 7106.8 |
| 20–35 | 22.8 | 16.2 | 1.37 | Elevation [m] | 1,310 | 2,010 | 3,435 |
| 35–50 | 26.7 | 3.0 | 0.01 | Longitude [°] | −114.1 | −123.1 | +99.2 |
| 50–65 | 26.6 | 0.6 | 0.00 | | | | |
| >65 | 5.5 | 0.0 | 0.00 | Latitude [°] | 48.2 | 46.9 | 35.78 |
| Total | 100.0 | 100.0 | 100.0 | | | | |

**Table 4** Percent distribution of watershed areas by aspect

| Aspect | Percent area cover | | | Description |
|---|---|---|---|---|
| | Tuchuck | Tenderfoot | Dashui | |
| <0 | 0.2 | 2.5 | 51.37 | Flat |
| 0–22.5 | 5.8 | 7.6 | 2.35 | North |
| 22.5–67.5 | 22.1 | 11.5 | 5.98 | Northeast |
| 67.5–112.5 | 16.7 | 6.4 | 5.05 | East |
| 112.5–157.5 | 7.9 | 12.7 | 5.11 | Southeast |
| 157.5–202.5 | 10.5 | 12.7 | 7.70 | South |
| 202.5–247.5 | 23.9 | 9.2 | 7.86 | Southwest |
| 247.5–292.5 | 3.2 | 12.9 | 6.84 | West |
| 292.5–337.5 | 4.6 | 18.1 | 2.25 | Northwest |
| 337.5–360 | 5.1 | 6.4 | 0.00 | North |
| Total | 100.0 | 100.0 | 100.0 | |

used as warm-up period for model parameters. Additional input datasets required by the PIXEL snowmelt scenario, such as elevation, slope and aspect of each pixel in the watershed, were extracted from the DEM of the corresponding watershed. In addition, information about the vegetation height ($h_0$) for different land covers (as required by the SNOWBP snowmelt module) was obtained directly from the SWAT database under crop data file, which are primarily used to calculate PET under the default SWAT model. Wind speed data at elevations other than where wind speed measurements were made were interpolated using the logarithmic wind function (Allen et al. 1998). The datasets were corrected for anomalies wherever encountered by cross checking for errors and substituting missing values.

### 2.3 Statistical Analysis

The statistical analyses in this manuscript were made based on the following comparisons: (a) the performance of each snowmelt module against observed historical data (predicted vs observed), (b) the performance of default snowmelt module against the SNOWBP (using elevation band approach) module (SWAT2K vs BAND), and (c) the performance of two snowmelt computation approaches using energy budget approach—SNOWBP (BAND vs PIXEL). Under “b” (i.e., SWAT2K vs BAND), the cause for discrepancy in the estimated snowmelt values is merely the method of snowmelt calculation (temperature-index vs energy-budget approach) since both methods employ snowmelt estimation on the basis of elevation bands. Whereas, under “c” (i.e., BAND vs PIXEL), the difference between estimated snowmelt

**Table 5** Sources of input data for the US watersheds (Tuchuck Creek and Tenderfoot)

| Data type | Sources |
|---|---|
| Soils | http://www.ncgc.nrcs.usda.gov/products/datasets/statsgo/data/index.html (STATSGO—1:250,000) |
| Land use/land cover | http://www.mrlc.gov/zones/zones_info.asp (NLCD—30 m horizontal grid) |
| Topography | http://data.geocomm.com/catalog/US/sublist.html (DEM—1:24,000) |
| Weather data | http://lwf.ncdc.noaa.gov/oa/ncdc.html (NCDC—precipitation, temperature, solar radiation, relative humidity) |
| Stream flow | http://waterdata.usgs.gov/nwis/rt (USGS—daily stream flows at the gauge stations) |

values is mainly because of the adjusting factors in the calculation of the incoming solar radiation on the basis of surface inclination (aspect and slope).

We employed various commonly used statistical tests in hydrology (Nash and Sutcliffe 1970; Krause et al. 2005) to compare the performances of these snowmelt modules in the SWAT model (the spearman correlation coefficient, Nash-Sutcliffe model efficiency coefficient, and runoff as percentage of rainfall). We have also estimated other sample statistics and measure of data distribution, such as mean, max, and standard deviation. We ran the statistical analyses using datasets from all three watersheds. Runoff data (both observed and simulated) for the period over which snowfall/snowmelt is expected (February through May for Tuchuck and Tenderfoot watersheds, and March through June for Dashui watershed) were selected to perform the statistical analyses.

## 3 Results and Discussions

Table 6 presents comparisons of performances between the default SWAT2K and SNOWBP (BAND and PIXEL) snowmelt modules using dataset from both the US and Chinese watersheds. According to Table 6,the snowmelt module represented by the default SWAT2K better reproduced the historical runoff data, compared with the SNOWBP module (BAND and PIXEL). Values of the correlation ($r = 0.91$, 0.78 and 0.78 at Tuchuck Creek and $r = 0.82$, 0.70, and 0.73 at Dashui watershed using SWAT2K, BAND and PIXEL snowmelt procedures, respectively) and Nash-Sutcliffe model efficiency coefficients (NS = 0.73, 0.50, 0.59 at Tuchuck Creek and NS = 0.66, 0.50, and 0.54 at Dashui watershed using SWAT2K, BAND and PIXEL snowmelt procedures, respectively) indicate that the default SWAT2K snowmelt estimation procedure better mimicked the historical runoff data. Similar statistical results (superior performance of the SWAT2K model over the other methods) were also observed at Tenderfoot watershed (Table 6). Other statistical descriptions, such as maximum, mean and total runoff as percent of total rainfall also substantiate similar claim that the SWAT2K snowmelt module better mimicked the historical runoff data at all three watersheds (Table 7).

On the other hand, comparing the statistical values corresponding with BAND and PIXEL snowmelt estimation methods (Table 6), the fact that an adjustment factor was accounted for in the computation of incoming solar radiation as a function of land surface inclination (slope and aspect—the SWIFT algorithm) produced relatively better results. We observed the Nash-Sutcliffe model efficiency coefficients of NS = 0.50 and 0.59 at Tuchuck Creek, and NS = 0.50 and 0.54 at Dashui watershed using the BAND and PIXEL methods, respectively. Similar results are depicted in Table 6 regarding the superior performance of the PIXEL method vis-à-vis the BAND method for Tenderfoot watershed. Also, from Table 6 (comparing BAND against PIXEL at the three watersheds), the PIXEL method performed better at the Tuchuck Creek (NS = 0.59) than at the other two watersheds (NS = 0.54 and 0.48 at Tenderfoot and Dashui watersheds, respectively).

Close scrutiny of the slope and aspect distributions of the watersheds (Tables 3 and 4) revealed that the majority of Tuchuck Creek watershed has steeper slopes (about 59% of the area having slope steepness >35°), which largely influences the adjusting factor for incoming solar radiation (Eq. 28). On the other hand, Tenderfoot and

**Table 6** Statistical comparison between historical and simulated runoff data following different snowmelt computation modules in the SWAT model at three watersheds

| Statistical | SWAT2K vs observed | | | BAND vs observed | | | PIXEL vs observed | | |
|---|---|---|---|---|---|---|---|---|---|
| parameters | Tuchuck | Tenderfoot | Dashui | Tuchuck | Tenderfoot | Dashui | Tuchuck | Tenderfoot | Dashui |
| Correlation coefficient | 0.91 | 0.60 | 0.82 | 0.78 | 0.54 | 0.70 | 0.78 | 0.58 | 0.73 |
| Nash-Sutcliffe model efficiency coefficients | 0.73 | 0.49 | 0.66 | 0.50 | 0.33 | 0.50 | 0.59 | 0.48 | 0.54 |
| | BAND vs SWAT2K | | | PIXEL vs BAND | | | | | |
| | Tuchuck | Tenderfoot | Dashui | Tuchuck | Tenderfoot | Dashui | | | |
| Correlation coefficient | 0.67 | 0.59 | 0.55 | 0.69 | 0.58 | 0.61 | | | |
| Nash-Sutcliffe model efficiency coefficients | 0.45 | 0.42 | 0.45 | 0.55 | 0.43 | 0.47 | | | |

SWAT2K, BAND and PIXEL are snowmelt estimation modules following simple temperature-index (SWAT2K) and process-based approaches (BAND and PIXEL, computed based on elevation band and pixel with the SWIFT algorithm, respectively). Data for Tuchuck (from 1986 to 1988), Tenderfoot (from 1996 to 2000) and Dashui (from 1992 to 1998) watersheds were used in these analyses

**Table 7** Sample statistics and measure of data distribution of historical and simulated runoff data following different snowmelt computation modules in the SWAT model at three watersheds

| Snowmelt module/ watershed | Observed | | | SWAT2K | | |
|---|---|---|---|---|---|---|
| Statistics | Tuchuck | Tenderfoot | Dashui | Tuchuck | Tenderfoot | Dashui |
| %RF | 69.0 | 58.0 | 23.0 | 67.0 | 48.0 | 30.0 |
| Max [$m^3/s$] | 5.8 | 4.0 | 114.0 | 7.2 | 6.0 | 122.0 |
| Ave [$m^3/s$] | 1.3 | 0.3 | 25.3 | 1.2 | 0.3 | 36.4 |
| STD [$m^3/s$] | 1.2 | 0.6 | 18.9 | 1.3 | 0.4 | 27.8 |
| | BAND | | | PIXEL | | |
| | Tuchuck | Tenderfoot | Dashui | Tuchuck | Tenderfoot | Dashui |
| %RF | 63.0 | 47.0 | 37.0 | 65.0 | 45.0 | 26.0 |
| Max [$m^3/s$] | 8.7 | 7.0 | 167.0 | 11.5 | 13.5 | 155.0 |
| Ave [$m^3/s$] | 0.79 | 0.3 | 58.9 | 1.1 | 0.3 | 23.5 |
| STD [$m^3/s$] | 1.17 | 0.4 | 56.1 | 1.5 | 0.8 | 21.9 |

SWAT2K, BAND and PIXEL are snowmelt estimation modules following simple temperature-index (SWAT2K) and process-based approaches (BAND and PIXEL, computed based on elevation band and pixel with the SWIFT algorithm, respectively). Where %RF is runoff as percent of total rainfall; Max, Ave and STD are sample maximum, average and standard deviations, respectively. Data for Tuchuck watershed (from 1986 to 1988), Tenderfoot (from 1996 to 2000) and Dashui (from 1992 to 1998) were used in these analyses

Dashui watersheds have flatter slopes with 80% and 99%, respectively, of their total areas having slopes less than 20° steepness, which minimally affects the adjusting factor in Eq. 28. That means, with other parameters being constant, the effect of using the PIXEL method over the BAND approach would not be significant since the adjustment factor's value (Eq. 28) is close to one. Yet, the overall improvement achieved by incorporating slope and aspect (PIXEL method) in the energy-budget approach for snowmelt estimation over the BAND approach was not large enough to render the results from the PIXEL method statistically superior (Table 6).

Although the snowmelt computation following the energy-budget approach is a physically based one, compared to the simple temperature-index method (SWAT2K), the results observed by this study confirm otherwise. Different justifications could be offered as to why SWAT2K better performed than the presumably process-based BAND and PIXEL approaches: (a) in the SNOWBP snowmelt module, most coefficients in Eqs. 5 through 29 are hard-coded based on global literature values and were not allowed to be modified during calibration except under very few occasions (Table 2) with most sensitive parameters. Thus, calibration efforts did not bring about significant changes in the final snowmelt estimation.

Conversely, in the snowmelt estimation approach using temperature-index (SWAT2K), all coefficients in Eqs. 2 to 4 are calibration coefficients, and thus their values were easily adjusted for different SWAT runs, resulting in good chances of correctly reproducing the historical data (Table 1); (b) because of the large number of parameters included in the energy-based snowmelt estimation equations, as opposed to the simple temperature-index equation, it is apparently possible for the errors to be propagated and compounded, and finally leading to unjustifiable deviation from observed historical phenomenon; and (c) it could also be possible that in the default SWAT2K snowmelt module all the physics of energy balance at the ground surface in each elevation band is very well accounted for by only those two parameters—

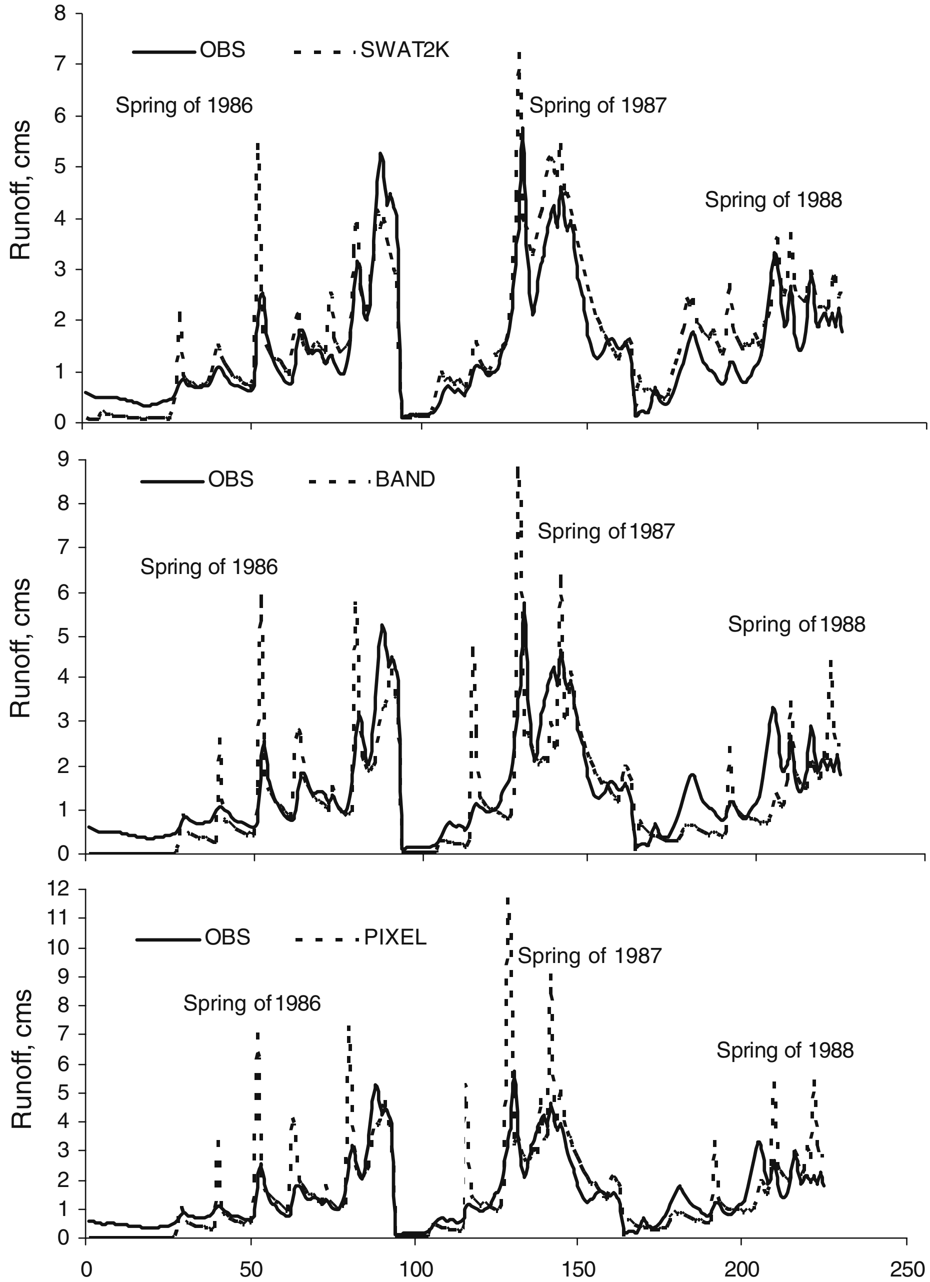


**Fig. 3** Measured (*OBS*) and simulated runoff using default SWAT2000 (*SWAT2K*) and process-based SNOWBP (*BAND* and *PIXEL*) snowmelt modules at the Tuchuck Creek watershed, USA. The *x*-axis is a serial number counting the number of days starting from the first day of snowfall to the end day of snowmelt season (usually from February through May) for years from 1986 through 1988

temperature and snowmelt rate indices—when appropriate parameters' values were used. In other words, it may be possible that the net solar radiation (a good proxy of air temperature) is the dominant energy flux driving snowmelt processes in areas studied, as opposed to rain-on-snow phenomenon, which is mainly dominated by sensible and latent heat fluxes—mostly controlled by temperature and humidity gradients and wind speed. Nevertheless, it should not be overlooked that the process-based snowmelt estimation models are used with little calibration as opposed to simpler temperature-index models, which should be vigorously calibrated against observed historical data, which in turn requires historical data from many years to reproduce observed results. For example, we noted that better performances were achieved by employing the SNOWBP module (both BAND and PIXEL), compared to the SWAT2K module under all three watersheds when SWAT was run

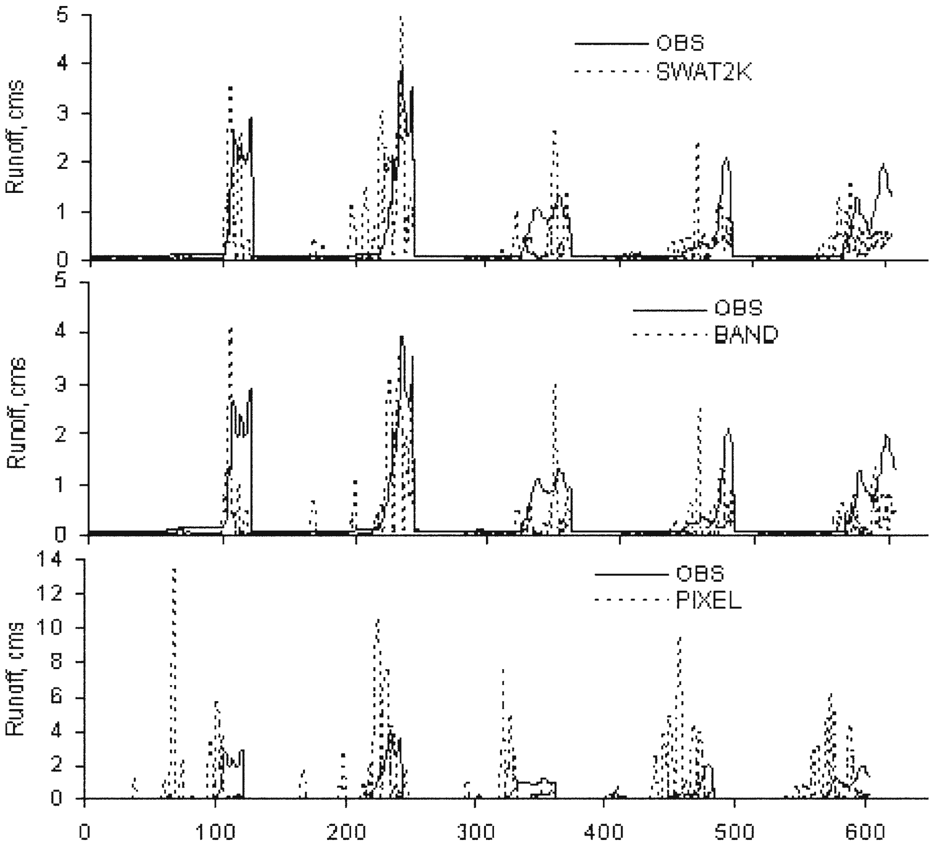


**Fig. 4** Measured (*OBS*) and simulated runoff using default SWAT2000 (*SWAT2K*) and process-based SNOWBP (*BAND* and *PIXEL*) snowmelt modules at the Tenderfoot watershed, USA. The $x$-axis is a serial number counting the number of days starting from the first day of snowfall to the end day of snowmelt season (usually from February through May) for years from 1996 through 2000

under default snowmelt parameters' values for each model (i.e., without parameters calibration) (not shown here for brevity).

Better performances by the default SWAT2K snowmelt module at Tuchuck Creek, Tenderfoot and Dashui watersheds are also depicted in Figs. 3, 4 and 5, respectively. The most striking results observed from comparing the performance of each snowmelt model under Figs. 3, 4 and 5 are that they all exhibit similar trends. Plots representing the SWAT2K, BAND and PIXEL snowmelt modules under Figs. 3, 4 and 5 show similar trends of increasing or decreasing with respect to some specific time on the *x*-axis. All the above results and accompanying discussions lead to a very interesting argument: this complex, process based model doesn't perform better than simpler and less demanding equations under some practical applications.

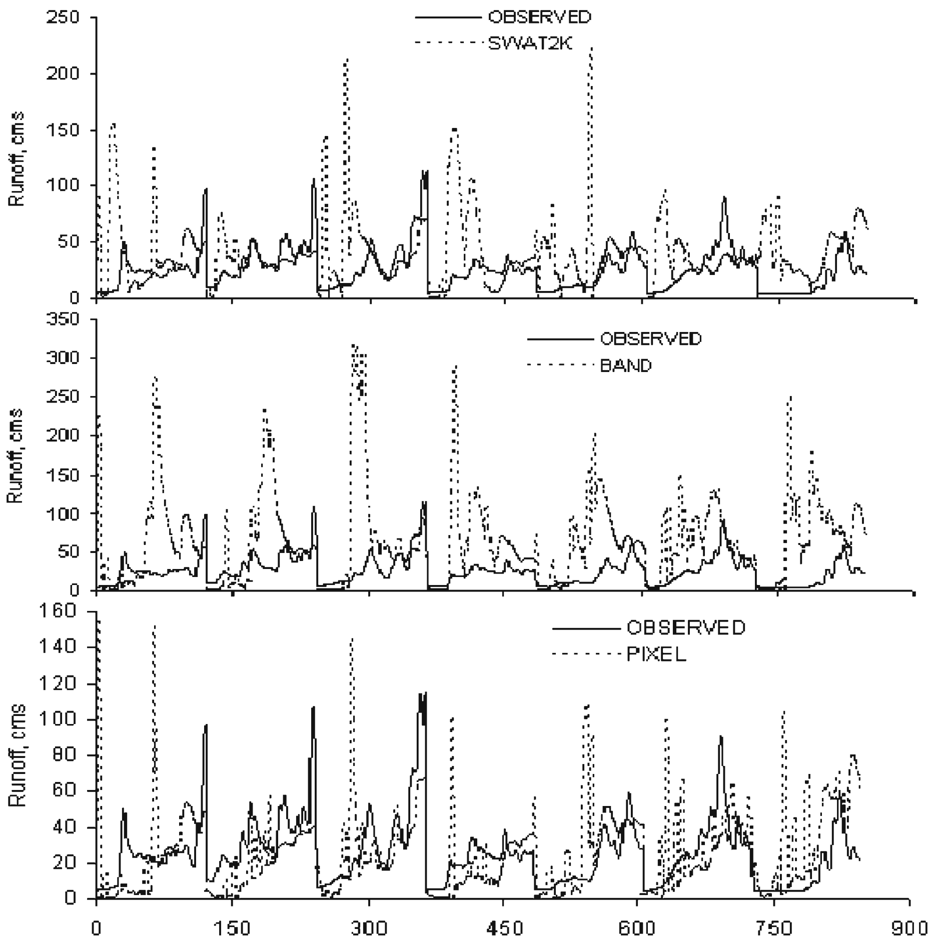


**Fig. 5** Measured (*OBS*) and simulated runoff using default SWAT2000 (*SWAT2K*) and process-based SNOWBP (*BAND* and *PIXEL*) snowmelt modules at the Dashui watershed, China. The *x*-axis is a serial number counting the number of days starting from the first day of snowfall to the end day of snowmelt season (usually from March through June) for years from 1992 through 1998

Similar claims have been made in the past by other researchers as well (Walter et al. 2005). In their study, Walter et al. (2005) observed comparable snowmelt results estimated using an even simpler temperature-index equation than we adopted in our study, compared to the process-based energy budget approach. Such observations apparently state that a simple temperature-index equation accompanied by well-established snowmelt rate coefficients is reliable and sufficient for some practical applications in snowmelt hydrology.

## 4 Conclusions

We performed detailed comparisons of two snowmelt estimation procedures (the default SWAT2K and SNOWBP). Our results demonstrated that the default SWAT2K model better mimicked observed historical runoff data consistently at all three studied watersheds, compared with the process-based energy budget SNOWBP approach. Although physically based models are more dependable given that less calibration efforts are required and could easily be applied to new sites, it is also possible for less detailed equations to perform just as equal or sometimes even better, as was noted from our results in this study. The justification could be that the temperature-index based snowmelt estimation on the basis of elevation band is good enough to account for all the physics of snowmelt processes given the calibration parameters are well adjusted, and more importantly that net solar radiation is the dominant driving energy for snowmelt with minimum effect from sensible and latent heat fluxes. It is also equally likely that the physically based model(s) need more options to adjust parameters if the global default values that were used in our analyses are not appropriate for the catchments involved.

On the other hand, the comparison within the SNOWBP approach (BAND vs PIXEL) corroborated the theoretical assumption that solar radiation varies not only based on latitude and altitude of the land surface but also based on land surface inclinations (aspect and slope). Yet, the improvements gained by employing the SWIFT algorithm (PIXEL) over the elevation band (BAND) approach were not significant. Thus, we conclude that for some practical applications, a simpler temperature-index snowmelt estimation model accompanied by well-established snowmelt rate coefficients is sufficient. However, whereas such models are good enough in areas where snowmelt processes are driven by local energy balances, it is insufficient in regions such as maritime areas where snowmelt processes are driven by turbulent transfers leading to rain-on-snow scenarios.

**Acknowledgements** We would like to extend our thanks to Mr. Flynn (Montana Department of Environmental Protection), Mr. Rob (University of Montana), and Mr. Zhang (graduate student at Texas A&M University) for providing the datasets for Tuchuck Creek, Tenderfoot, and Dashui watersheds, respectively. Ms. Kim Davis of Texas A&M University wrote the ArcGIS scripts to help extract slope, elevation and aspect ASCII files required in the SNOWBP (PIXEL) module. We would also like to sincerely thank the two anonymous reviewers and editor for their detailed review and excellent contributions towards the improvement of this manuscript.

## References


Albert MR, Krajeski GN (1998) A fast physical based point snowmelt model for distributed application. Hydrol Process 12:1809–1824

Allen RG, Periera LS, Raes D, Smith M (1998) Crop evapotranspiration; guidelines for computing crop water requirements. FAO irrigation and drainage paper. Rome, Italy, No. 56, p 300

Anderson E (1968) Development and testing of snow pack energy balance equations. Water Resour Res 4(1):19–37

Anderson EA (1973) National weather services river forecast system—snow accumulation and ablation model. NOAA Tech. Memo. NWS-HYDRO-17, US Department of Commerce, Silver Springs, MD, p 217

Anderson EA (1976) A point energy and mass balance model of a snow cover. NOAA Tech. Rep. NWS 29, National Weather Service, Silver Spring, MD

Arnold JG, Williams JR, Srinivasan R, King KW (1996) SWAT manual. USDA Agricultural Service and Blackland Research Center, Temple, TX

Azien VB, Ezien EM, Melack JM (1996) Precipitation, melt and runoff in the northern Tien Shan. J Hydrol 186:229–251

Bathurst JC, Cooley KR (1996) Use of the SHE hydrological modeling system to investigate basin response to snowmelt at Reynolds Creek, Idaho. J Hydrol 175:181–211

Becker S (2001) Calculation of direct solar and diffuse radiation in Israel. Int J Climatol 21:1561–76

Bowen IS (1926) The ratio of heat losses by conduction and by evaporation from any water surface. Phys Rev 2(27):779–787

Brutsaert W (1982) Evaporation into the atmosphere: theory, history, and applications. Reidel, Dordrecht, p 299

Calder IR (1990) Evaporation in the uplands. Wiley, Chichester, p 148

Cazorzi F, Fontana DG (1996) Snowmelt modeling by combining air temperature and a distributed radiation index. J Hydrol 181:169–187

Choudhury BJ, Monteith JL (1988) A four-layer model for the heat budget of homogeneous land surfaces. Q J R Meteorol Soc 114:373–398

Debele B, Srinivasan R (2005) Comparison of the performances of temperature-index and process-based energy budget snowmelt estimation approaches in the SWAT model. Texas A&M University, Spatial Sciences Laboratory, College Station, TX, p 40

Debele B, Srinivasan R, Parlange JY (2007) Accuracy evaluation of weather data generation and disaggregation methods at finer timescales. Adv Water Resour 30(5):1286–1300. doi:10.1016/j.advwatres.2006.11.009

Essery R (2003) Aggregated and distributed modeling of snow cover for a high-latitude basin. Glob Planet Change 38:115–120

Gray D, Male D (1981) Handbook of snow. Elsevier, New York, p 776

Gray DM, Prowse TD (1992) Snow and floating ice. In: Maidment DR (ed) Handbook of hydrology. McGraw-Hill, Inc., New York, pp 7.1–7.58

Green HM, Kozek AS (2003) Modeling weather data by approximate regression quantiles. ANZIAM 44(E):C229–C248

Hargreaves GH, Samani ZA (1985) Reference crop evapotranspiration. Appl Eng Agric 1(2):96–99

Herzfeld M (1996) Sea surface temperature and circulation in the Great Australian Bight. Ph.D. Thesis, School of Earth Science, Flinders University, South Australia

Hodges B (1998) Heat budget and thermodynamics at a free surface: some theory and numerical implementation (revision 1.0c) ED 1300 BH. Center for Water Research, University of Western Australia, p 14

Imberger J, Patterson JC (1981) A dynamic reservoir simulation model—DYRESM: 5. In: Fiescher HB (ed) Transport models for inland and coastal waters. Academic, San Diego, pp 310–361

Koivusalo H, Kakkonen T (2002) Snow processes in a forest clearing and in a coniferous forest. J Hydrol 262:145–164

Koivusalo H, Heikinheimo M, Karvonen T (2001) Test of a simple two-layer parameterization to simulate the energy balance and temperature of a snow pack. Theor Appl Climatol 70:65–79

Krause P, Boyle DP, Base F (2005) Comparison of different efficiency criteria for hydrological model assessment. ADGEO 5:89–97

LaMalfa EM, Ryle R (2008) Differential snowpack accumulation and water dynamics in aspen and conifer communities: implications for water yield and ecosystem function. Ecosystems 11(4):569–581. doi:10.1007/s10021-008-9143-2

Link T, Marks D (1999) Distributed simulation of snowcover mass- and energy-balance in the boreal forest. Hydrol Process 13(14–15):2439–2452
Lundberg A, Calder I, Harding R (1998) Evaporation of intercepted snow: measurement and modeling. J Hydrol 206:151–163
Male DH, Granger RJ (1981) Snow surface energy exchange. Water Resour Res 17:609–627
Manohar A, Singh P, Goel NK, Singh RD (2008) Climate variability influences on hydrological responses of a large Himalayan basin. Water Resour Manag 22(10):1461–1475. doi:10.1007/s11269-007-9237-1
Marks D, Dozier J (1992) Climate and energy exchange at the snow surface in the alpine region of the Sierra Nevada: 2. Snow cover energy balance. Water Resour Res 28:3043–3054
Marks D, Kimball J, Tingey D, Link T (1998) The sensitivity of snowmelt processes to climate conditions and forest cover during rain-on-snow: a case study of the 1996 Pacific Northwest flood. Hydrol Process 12:1569–1587
Marks D, Domingo J, Susong D, Link T, Garen D (1999) A spatially distributed energy balance snowmelt model for application in mountain basins. Hydrol Process 13:1953–1959
Marshall S, Oglesby RJ, Maasch KA, Bates GT (1999) Improving climatic model representations on snow hydrology. Environ Model Softwa 14:327–334
Martinec J, Rango A, Roberts RT (2008) Snowmelt runoff model (SRM) user's manual. New Mexico State University, Las Cruces, New Mexico, p 175
McKay GA, Gray DM (1981) The distribution of snow. In: Gray DM, Male DH (eds) Handbook of snow. Pergamon, Toronto, ON, pp 153–190
McKenny DW, MacKey BG, Zavitz BL (1999) Calibration and sensitivity analysis of a spatially-distributed solar radiation model. Int J Geogr Inf Sci 11:457–97
Morid S, Gosain AK, Keshari AK (2001) Challenges in snowmelt-runoff simulation. J Earth Space Phys 27(2):11–20
Morid S, Gosain AK, Keshari AK (2002) Solar radiation estimation using temperature-based stochastic and artificial neural networks approaches. Nord Hydrol 33(4):291–304
Nash JE, Sutcliffe JV (1970) River flow forecasting through conceptual models, part I—a discussion of principles. J Hydrol 10:282–290
National Engineering Handbook (2004) Part 630 hydrology, chapter 11 (snowmelt). United States Department of Agriculture, Natural Resources Conservation Services
Neitsch SL, Arnold JG, Kiniry JR, Williams JR (2001) Soil and water assessment tool (SWAT) theoretical documentation. Blackland Research Center, Texas Agricultural Experiment Station, Temple, TX, p 781
Pomeroy JW, Toth B, Granger RJ, Hedstrom NR, Essery RLH (2003) Variation in surface energetics during snowmelt in a subarctic mountain catchment. J Am Meteorol Soc 4(4):702–719
Rango A, Dewalle D (2008) Snowmelt-runoff model (SRM). In: Dewalle D, Rango A, (eds) Principles of snow hydrology. Cambridge University Press, Cambridge, NY, pp 306–364
Rango A, Martinec J (2008) Predictions for snow cover, glaciers and runoff in a changing climate. In: Proceedings of International Interdisciplinary Conference on Predictions for Hydrology, Ecology, and Water Resource Management: Using Data and Models to Benefit Society. Prague, Czech Republic, 15–18 September, pp 277–280
Rasmus S, Gustafsson D, Koivusalo H, Lauren A (2008) Estimation of winter leaf area index and sky view fraction for snow modeling in boreal coniferous forests. American Geophysical Union, Fall Meeting 2008, abstract no. C34A-01
Sui J, Koehler G (2007) Impacts of snowmelt on peak flows in a forest watershed. Water Resour Manag 21(8):1263–1275. doi:10.1007/s11269-006-9080-9
Swift LW (1976) Algorithm for solar radiation on mountain slopes. WRR 12(1):108–112
Tanasienko AA, Chumbaev AS (2008) Features of snowmelt runoff waters in the Cis-Salair region in an extremely snow-rich hydrological year. Contemporary Problems of Ecology 1(6):687–696. doi:10.1134/S199542550806012X
Tarboton DG, Luce CH (1996) Utah energy balance snow accumulation and melt model (UEB), computer model technical description and users' guide. Utah Water Research Laboratory and USDA Forest Service Intermountain Research Station (http://www.engineering.usu.edu/dtarb/). http://citeseer.ist.psu.edu/tarboton96utah.html
Todini E (1996) The ARNO rainfall–runoff model. J Hydrol 175:339–382
US Army Corps of Engineers (1956) Snow hydrology. U.S. Army Corps of Engineers, North Pacific Division, Portland, Oregon, p 437
US Army Corps of Engineers (1960) Runoff from snowmelt (EM 1110-2-1406):68. U.S. Govt. Printing, Washington, DC

US Army Corps of Engineers (1998) Engineering and design-runoff from snowmelt (Engineering manual 1110-2-1406). US Army Corps of Engineers, Washington, DC

Valeo C, Ho CLI (2004) Modeling urban snowmelt runoff. J Hydrol 299:237–251

Walter MT, Brooks ES, McCool DK, King LG, Molnau M, Boll J (2005) Process-based snowmelt modeling: does it require input data than temperature-index modeling? J Hydrol 300:65–75

Wigmosta MS, Vail LW, Lettenmaier DP (1994) A distributed hydrology-vegetation model for complex terrain. Water Resour Res 30(6):1665–679

Wilson JP, Gallant JC (2000) Secondary topographic attributes. In: Wilson JP, Gallant JC (eds) Terrain analysis, principles and applications. Wiley, New York, pp 87–132

Zhang Y, Li B, Bao A, Zhou C, Chen X, Zhang X (2007) Study on snowmelt runoff simulation in the Kaidu River basin. Sci China Earth Sci 50(1):26–35. doi:10.1007/s11430-007-5007-4

Zhao Q, Liu Z, Li M, Wei Z, Fang S (2009) The snowmelt runoff forecasting model of coupling WRF and DHSVM. Hydrol Earth Syst Sci Discuss 6:3335–3357